Manuscript refereed by Dr Bernhard Tabernig (Plansee SE, Austria)

3D Screen Printing for the Fabrication of Small Intricate Ti-6Al-4V Parts

Marie Jurisch, Thomas Studnitzky, Olaf Andersen, Bernd Kieback
Fraunhofer Institute for Manufacturing Technology and Advanced Materials, Branch Lab Dresden, Germany
marie.jurisch@ifam-dd.fraunhofer.de

ABSTRACT
For the production of complex shaped titanium parts huge advances have been made by powder metallurgy (P/M) during the last years. However, when it comes to miniaturized parts with intricate inner structures like closed channels without entrapped powder and high aspect ratios conventional P/M methods are stretched to their limits. To remedy this shortcoming, Fraunhofer IFAM Dresden uses 3D screen printing, a modified screen printing process based on a powder-binder mixture which is printed layer-by-layer to the desired shape followed by debinding and a conventional sintering step. Especially for small parts a productivity of several million parts per year is achievable. The objective of this work is to demonstrate the possibility to manufacture complex designs based on titanium including thin walls down to 120 µm. Therefore, pre-alloyed gas atomized Ti-6Al-4V powder was used. Analysis of part accuracy, resulting porosity, impurity level and mechanical properties were performed.

INTRODUCTION
For the manufacturing of intricate titanium parts near-net-shape technologies like metal injection molding (MIM) or selective laser melting (SLM) are beneficial as they overcome the high costs for the difficult workability and the huge amounts of waste material. However, the lack of mass production capability [1], limited surface qualities and feature sizes in the case of SLM and limited aspect ratios (ratio of feature depth to width) and expensive tools for MIM [2] led to the development of the new technology of 3D screen printing. This method is derived from the conventional two dimensional screen printing known for the production of silicon solar cells, gas sensors, piezoelectric and other electronic devices [3, 4]. It combines the principles of MIM and additive manufacturing as it is a layer-by-layer process. 3D screen printing is suitable for manufacturing of intricate small parts with complex inner shapes. The ability for industrial scale production of more than 1.000.000 parts per year for part sizes of 5 x 5 x 5 mm makes the 3D screen printing a competitive and cost effective method. The surface roughness is between that of MIM and additive manufacturing. However, the use of fine powders and organic binders make 3D screen printing of titanium a challenging task due to the high affinity of titanium to especially oxygen, which lead to a degradation of the mechanical properties of titanium [5]. As many researchers deal with these problems some efforts have been made to improve the impurity levels of MIM parts [6-9]. These measures might also be useful for 3D screen printing of titanium.

The 3D screen printing process includes four steps (Figure 1). In the beginning a screen layout has to be derived by slicing of the virtual part design. Changes in the chosen printing direction of the geometry have to be expressed by different screens.
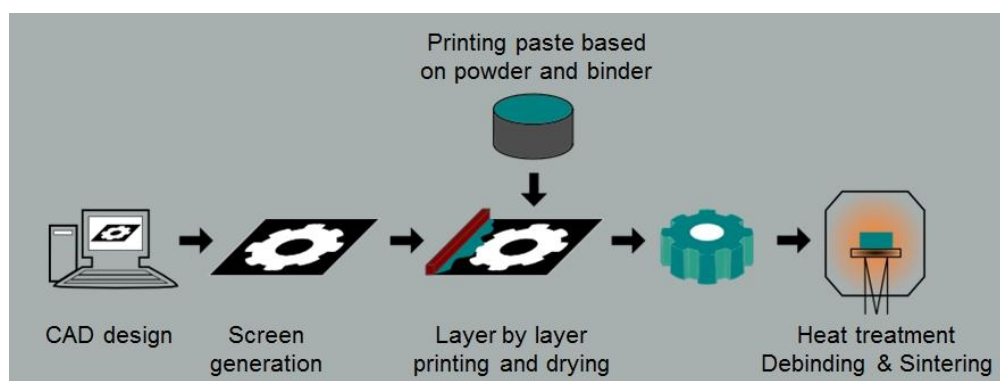

Figure 1: Principle of the 3D screen printing process

The next step is the mixing of powders, binder and additives to a homogenous printing paste. With the help of printing squeegees the paste is pressed through the screen on a substrate forming a first layer

of the desired layout which will be dried before printing of the next layers. The steps of printing and drying have to be repeated until a certain part height is reached. This might reach up to several centimeters. By a change of the screen layout during printing, dimensional changes including complex inner shapes like closed channels (flow fields) or overhangs can be achieved.

The printed line characteristics are influenced by paste viscosity, homogeneity, particle size and distribution, solid loading, and surface tension. Furthermore, it is associated with printing parameters such as substrate adhesion, squeegee rate, kind and pressure, off-contact distance, screen parameters (emulsion thickness, screen tension, mesh opening and thread diameter).

The printing is finally followed by a heat treatment based on binder removal and sintering.

EXPERIMENTAL

Materials. The metal powder used in the present study is gas atomized, pre-alloyed Ti-6Al-4V powder supplied by TLS, Germany. The powder provides a medium particle size of 12 µm and a spherical shape. The characteristics of the Ti-6Al-4V powder are shown in Table 1.

Table 1: Characteristics of the starting Ti-6Al-4V powder.

Powder type	Medium particle size [µm]	Particle size d90 [µm]	BET surface [m²/g]	Impurities [wt.-%]		
				O	C	N
Ti-6Al-4V	12	22	0,18	0,206	0,011	< 0,005

The binder is organic and water soluble, providing easy handling and environmental friendliness. Additionally, in order to influence the printing behavior a surfactant, plasticizer and defoaming agents were used to guarantee a homogenous and lasting printing paste. For the adjustment of a good flowability the binder, solvents and additives should provide particle wetting, dispersion stability and homogeneity of the paste. They also determine a special rheological behavior that allows paste flow through the screen mesh during printing and a proper adhesion to the substrate without spreading. Finally, it regulates the paste drying during and after printing. For minimal contaminations, the binder and additives should not react with the screen materials or the substrate and with the powder particles and should be easily debindered with low ashes content.

Printing Paste formulation. The shear rate dependency of the paste viscosity is a critical factor for a high part quality. The paste must show a distinct pseudoplasticity to assure a fast filling and emptying of the mesh on the one hand. Additionally, the paste has to be thixotropic so that it is able to merge below the mesh fibers during printing. This will allow the film levelling and filling the irregularities and voids. On the other hand, the printed paste also has to recover to elastic behavior fast enough to enable good edge definitions on the substrate without running of the paste. Three different binder proportions were examined in this study to investigate the influence of the rheological behavior on the part quality. The printing pastes were obtained with a powder loading of 38, 43 and 48 vol.-%, respectively by changing the amount of binder (Table 2).

Table 2: Composition of the examined printing pastes.

Printing paste	Binder content [wt.-%]	Additives [wt.-%]	Powder loading [wt.-%]	Powder loading [vol.-%]
B1	24,8	1,7	73,5	38
B2	20,8	1,8	77,3	43
B3	17,5	1,9	80,6	48

The powder was mixed with binder and additives and dissolved in a vacuum dispenser from Pendraulik and a speedmixer from Hauschild for 20 min with a mixing speed of 1000 rpm at room temperature. The resulting pastes were homogeneous without air inclusions or sedimentation. For 3D screen printing, the paste is used at room temperature what is different compared to binder systems for MIM.

Printing process. Appropriate printing parameters were chosen and kept constant for the printing of each paste. The part and layer height were measured by a laser system.

The screen (Koenen GmbH, Germany) had the following characteristics: mesh opening w = 54 µm, thread diameter d = 23 µm, open area a_0 = 49 % and screen layout dimensions of about 210 x 290 mm. The parts were printed on two different substrate materials ceramic (B2) and polyethylene-foil (B1). The printing was carried out under room temperature on a special 3D screen printing machine.

For each pastes 20 layers were printed with the same printing parameters and drying times.

Heat treatment. Thermal debinding was carried out under flowing argon in a tube furnace with a heating rate of 5 K/min and several holding times in order to remove binder and additives. The maximum temperature for debinding was 823 K held for 1 hour. The parts were transferred on a tungsten sintering aid to guarantee no further oxygen pick-up during heat treatment. The sintering was conducted under high vacuum with a heating and cooling rate of 10 K/min up to 1523 K. The sintering time was 1 hour.

Microstructural and rheological characterization. The printing process is executed at room temperature in air on an open screen printing machine. A plate-plate rheometer from Thermo Scientific was used to measure the viscosities of the printing pastes during shear loading. The jump test describes the process steps of paste supply, mesh filling, paste at rest, printing (mesh emptying) and finally drying of the printed structures. The associated shear rates for flooding and printing are 100 s^{-1} and 1000 s^{-1}. For the relaxing sequences between the squeegee strokes the shear rate was held at 0.1 s^{-1}.

Chemical analyses were made to examine the contaminations by oxygen, carbon and nitrogen in the as-received powder, within paste and the debindered and sintered titanium alloy parts.

For microscopy, specimens were ground and polished mechanically. Microscopic investigations were carried out to determine the porosity, pore size and microstructure of the titanium alloy parts and the development of minimum structural features and line precision depending on the printing paste.

Tensile tests and micro hardness measurements were carried out in order to examine first mechanical properties of the resulting sintered parts. Flat tensile test specimens were screen printed, sintered and measured without any post processing.

RESULTS AND DISCUSSION

Rheological behavior. Figure 2 illustrates the different viscosities during the simulated printing process. All three pastes show a distinct shear thinning behavior.

Paste B3 is not suitable for 3D screen printing, as the binder network is breaking down during shearing. The reason is a too high powder loading for the given binder and additives that results in attrition of the binder by the powder particles. This is illustrated by the decrease in viscosities at rest for paste B3 after the second step of shearing (1000 s^{-1}) compared to the stage before shearing (Fig. 2). During further printing steps it loses its shear thinning behavior. For this reason paste B3 will not be considered in the following sections any more.

The other two pastes show a full recovery at rest. Paste B2 is thereby showing the greatest pseudoplasticity which was calculated using the Herschel-Bulkley model [10]. The related flow indexes for pastes B1 and B2 are 0.43 and 0.39, respectively. Paste B2 shows higher static viscosities compared to B1 due to a higher powder loading (Fig. 2). Paste B1 exhibits a very small thixotropy which could lead to the formation of defects and voids as the paste has not enough time for levelling (Fig. 2). Also a decrease in elastic behavior compared to B2 was measured by other rheological tests. This could result in smudging the paste underneath the screen.
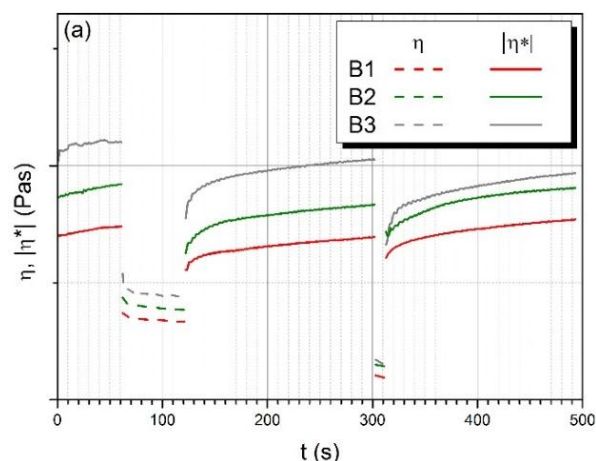

Figure 2: Jump test for simulating the rheological behaviour of the printing pastes B1, B2 and B3 during screen printing steps, η viscosity during shearing and |η*| complex viscosity at rest

Optical characterization of the printed structures. Besides the rheological aspects the

printing process itself has a strong influence on the part quality. As well as heating and cooling rates during the drying steps the squeegee pressure, kind and speed are important factors that can lead to the development of pores, rough surfaces, insufficient line qualities or broken lines [11]. Moreover, the mesh and emulsion quality strongly affect the line accuracy (see Fig. 3). Thus, rounded corners and uneven edges will be transferred onto the printed parts (Fig. 4). Because of the relatively large powder particles there is also a certain danger for the particles getting stuck in the openings of the mesh. The consequence is the formation of defects in the printed parts. Additionally, an inhomogeneity in pore distribution and a high bonding to the sintering substrate can cause anisotropic shrinkage.
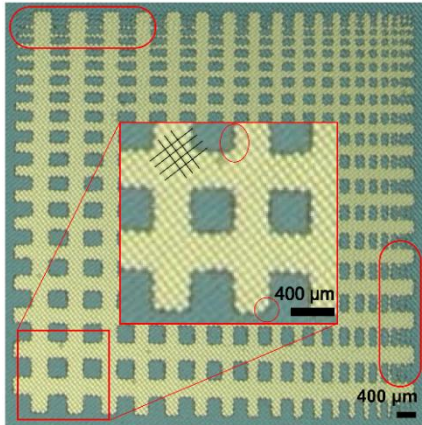

Figure 3: Test pattern on the screen, rounded corners, rough edges and unsatisfactory fine lines lead to associated printing quality.
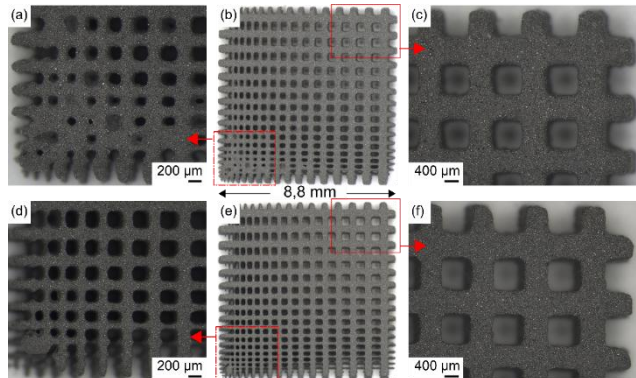

Figure 4: Comparison of the printed test patterns based on paste B1 (a-c) and B2 (d-f).

The printed structures based on the two different printing pastes B1 and B2 are shown in Figures 4. B2 provides a higher line accuracy and less printing porosity. The reason for the quality difference is the rheological development of the paste. While the paste B2 exhibits a good line definition, the paste B1 is often spread where closely connected edges and lines provide bridging and in the same time shows voids and a rough surface. Thus, levelling could not be finished as the poor thixotropic behavior causes a fast increase in static viscosity. Moreover, the spreading occurred as a result of a less distinct elastic behavior after shearing. This is illustrated by Figure 4 for the test pattern of paste B1. In areas with a greater line width (Fig. 4 c, f) there are no traces of quality change whereas the small gaps in Figure 4 a, d are partly filled and less defined compared to the results provided by paste B2. Both printing tests showed more or less void formation on compact surfaces. As some of the voids have been formed only after several layers, another reason for this is the loss of moisture in the pastes on the screen due to a non-encapsulated 3D printing machine which shifts the viscosities to a higher level. By holding a constant solvent content these problems could partly be solved.

More than 10 % of the powder particles are greater than 18 µm and therefore do not fit to the condition of at least 3 particles passing side by side through the screen openings of in this case 54 µm, which can lead to failures in the printed parts due to clogging of the mesh openings [12]. Hence, the screen used was not appropriate for the examined printing pastes. Besides poorly defined edges on the screen (Fig. 3), this is another reason for the bad accuracy of the test pattern edges in Figure 4.

The achieved line widths for both pastes according to Figure 4 are 120 to 400 µm and the finest feature size is about 120 µm. The averaged layer thickness was about 25 µm. As mentioned before, the interaction between 3D screen printing parameters, screen and substrate surface tension and paste rheology affect the printing results and also the layer thickness and have to be further examined.

Oxygen and carbon pick-up. The examined powder contaminations oxygen, carbon and nitrogen of the starting powder accounts 0.2, 0.08 and less than 0.05 wt.-% which is very high due to the handling after the atomization and the fine powder. Table 3 gives an overview of the impurity development during the process. To investigate a possible rise of impurities during printing, green parts were dissolved in water, put in an ultrasonic bath and the resulting powder was cleaned of binder and additives. The cleaned powder was again chemically analysed.

No changes in oxygen and nitrogen but partly in carbon were determined which is due to an unfinished cleaning or differing values of the starting powders. After debinding the parts exhibited a huge change in oxygen and carbon values of nearly 0.2 wt.-%. The results for the impurity levels after sintering indicate adequate nitrogen levels for the Ti-6Al-4V alloy, whereas the oxygen and carbon levels are much higher than the maximum levels tolerable according to the standard ASTM F 2885 for

MIM components for medical applications [13]. They are limited to 0.2 wt.-% oxygen and 0.08 wt.-% carbon. There is nearly no change in impurity levels after sintering compared to debinding values. Obviously, the major increase in impurities happens during debinding due to high amounts of oxygen and carbon in the binder. Prospectively, efforts have to be made in case of binder compositions, solvent debinding, increase of powder loadings and thermal debinding process optimization.

Table 3: Oxygen, carbon and nitrogen pick-up during the 3D screen printing process and heat treatment.

Processing step	Impurities [wt.-%]		
	O	C	N
As-received powder	0,206	0,011	< 0,005
Green structures (after 3D screen printing)	0,203	0,028	0,028
Brown structures (after debinding)	0,392	0,103	0,050
Sintered structures	0,411	0,114	0,057

Microstructure and mechanical properties. During sintering, a lamellar basketweave microstructure has developed. Figure 5 shows the microscopy of the test pattern in height direction. Lamellar colonies with different sizes are visible. The bright regions show the α-phase and the dark ones correspond to β-phase. Both α-colony size and the α-lath width are very large which will strongly affect the mechanical properties. Additionally, due to the high contents in oxygen and carbon, which act as α-stabilizing elements, and slow cooling rates, a large α-layer is formed around the former β-grain boundaries [14]. The measured maximum tolerance of the 3D screen printed structures is ± 30 μm for line thicknesses of 160 μm mostly due to printing errors or screen defects.
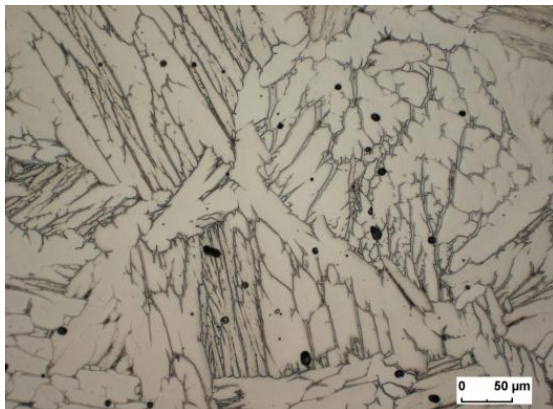

Figure 5: Microstructure of the screen printed Ti-6Al-4V test pattern in height direction with no signs of the printed layers.
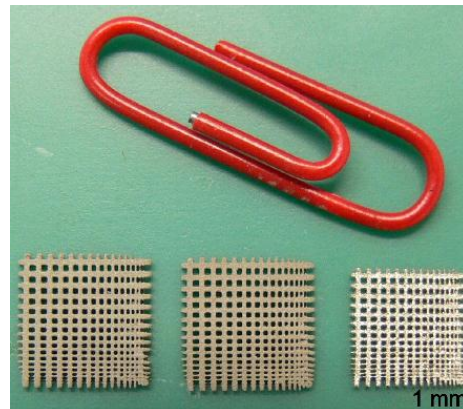

Figure 6: Comparison between green, debindered and sintered Ti-6Al-4V test patterns with a shrinkage of 11% after sintering.
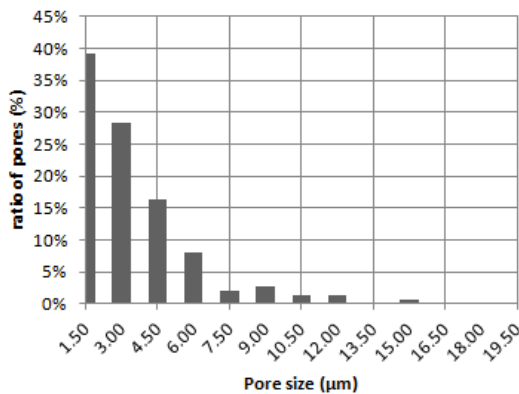

Figure 7: Pore size distribution of the sintered Ti-6Al-4V test pattern.

Table 4: Mechanical properties of 3D screen printed Ti-6Al-4V.

Max. pore size (μm)	YS [MPa]	UTS [MPa]	Hardness HV
< 15	762	828	400

The resulting pores are round shaped and the closed porosity is less than 1 % in the fine structures like the test pattern and at a maximum of 3 % for parts with compact surfaces (Fig. 5). This is due to

processing errors which produced additional pores mostly in compact areas. The related pore size distribution for the test pattern with small pores of less than 15 μm is given by Figure 7. No surface cracks or dimensional distortions could be observed. The lateral sintering shrinkage was measured to be 11 ± 1 %. A comparison of green and sintered structures is provided in Figure 6.

The results of the tensile and microhardness tests are provided in Table 4. Due to the high impurity content, the screen printed parts show a relatively high tensile strength and microhardness. The elongations are less than 1 %. This is in agreement with the literature, as an oxygen value higher than 0.3 wt.-% leads to a decrease in elongation [15, 16].

CONCLUSIONS AND OUTLOOK

3D screen printing proves to be a suitable method for printing intricate nearly dense parts with high quality features of less than 150 μm. The printing pastes itself showed to have a strong influence on the part quality and was found to be best for a powder loading of 43 Vol.-% for the used binder system. The screen was not appropriate for the used particle size distribution and the paste rheology changed during the process. Therefore, there is still a high potential for further miniaturization of printed structures, avoiding surface defects, and increasing accuracy and surface quality. A new 3D screen printing machine is currently being built up that is encapsulated and provides a large variety of adjustable printing parameters, as well as improved monitoring devices. A total impurity level of 0.5 wt.-% is not yet satisfactory and needs further investigation in order to reach grade 5 levels. In order to improve impurity content, a solvent debinding and an optimization of the thermal debinding will be examined which is expected to further reduce oxygen and carbon contents, resulting in higher elongations. Additionally, variations of the sintering process with regard to temperature and atmosphere will be investigated in order to reduce the width of α-laths and thus to improve mechanical properties.

REFERENCES
[1]   I. Gibson, D.W. Rosen, B. Stucker, Aditive Manufacturing Technologies. Rapid Prototyping to Direct Digital Manufacturing, Springer, 2010.
[2]   U.M. Attia, J.R. Alcock, A review of micro-powder injection moulding as a microfabrication technique, J. Micromech. Microeng. 21 (4) (2011).
[3]   D. Erath, A. Filipovic, M. Retzlaff, Advanced screen printing technique for high definition front side metallization of crystalline silicon solar cells, Solar Eneergy Materials & Solar Cells 94 (2010), 57-61.
[4]   S. Ito, P. Chen, P. Comte, Fabrication of Screen-Printing Pastes From TiO_2 Powders for Dye-Sensitised Solar Cells, Prog. Photovolt: Res. Appl. 15 (2007), 603-612.
[5]   E. Baril, L.P. Lefebvre and Y. Thomas, Interstitial elements in titanium powder metallurgy: sources and control, Powd. Metall. 54 (2011) 183-187.
[6]   A.T. Sidambe, F. Derguti, I.Todd, Metal Injection Moulding of Low Interstital Titanium, Key Engineering Materials 520 (2012), 145-152.
[7]   A.T. Sidambe, I.A. Figueroa, H.G.C. Hamilton, Metal injection moulding of Ti-64 components using a water soluble binder, PIM International 4 (2010) 56-62.
[8]   G. Shibo, Q. Xuanhui, H. Xinbo, Powder injection moulding of Ti-6Al-4V alloy, Journal of Materials Processing Technology 173 (2006), 310-314.
[9]   G. Wen, P. Cao, B. Gabbitas, Development and Design of Binder Systems for Titanium Metal Injection Moulding: An Overview, Metallurgical and Materials Transaction A: Physical Metallurgy and Materials Science, 44A (3) (2013), 1530-1547.
[10]   T.G. Mezger, The Rheology Handbook: For Users of Rotational and Oscillatory Rheometers, Vincentz Network, 2nd edition, 2006.
[11]   R. Faddoul, N. Reverdy-Bruas, A. Blayo, Formulation and screen printing of water based conductive flake silver pastes onto green ceramic tapes for electronic applications, Materials Science and Engineering B 177 (2012), 1053-1066.
[12]   P. Hahne, Innovative Drucktechnologien. Siebdruck-Tampondruck, Der Siebdruck, Lübeck, 2001.
[13]   Standard Specification for Metal Injection Molded Titanium-6Aluminum-4Vanadium Components for Surgical Implant Applications, Annual Book of ASTM Standards Standard F2885-11 (2011).
[14]   M. Peters, C. Leyens, Titan und Titanlegierungen, Wiley-VCH, Weinheim, 2002.
[15]   T. Ebel, O.M.Ferri, W. Limberg, Metal Injection Moulding of Advanced Titanium Alloys, Advances in Powder Metallurgy & Particulate Materials-2011, MPIF San Franscisco, Part 4 (2011).
[16]   D. Auzène, C. Mallejac, C. Demangel, Influence of surface aspects and properties of MIM titanium alloys for medical applications, PIM International 6 (2012), 61-65.